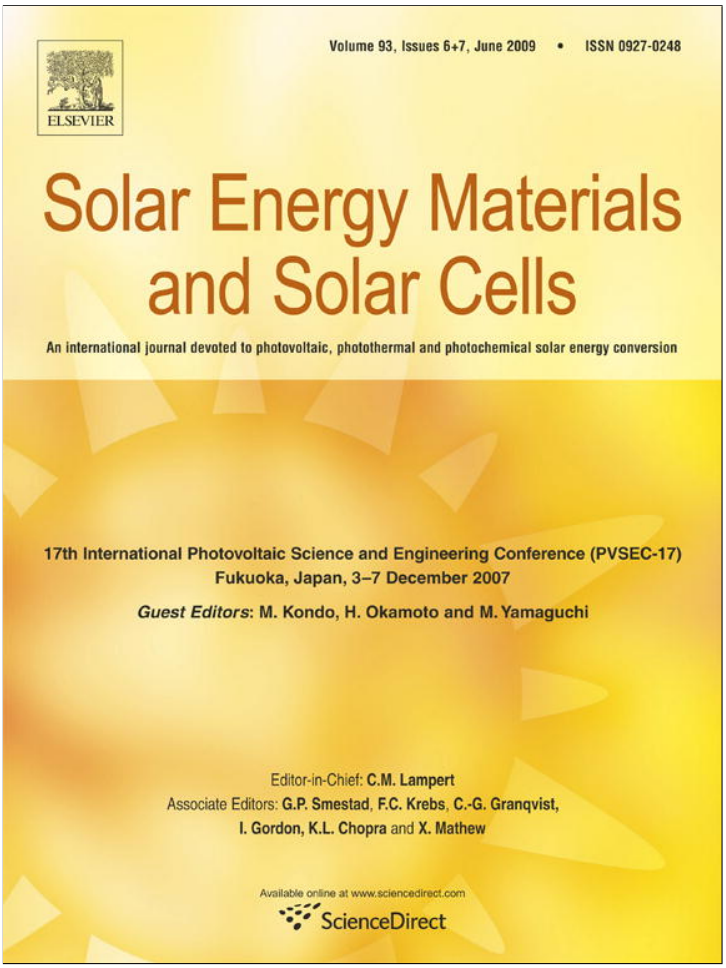

Solar Energy Materials & Solar Cells 93 (2009) 888–892

Contents lists available at ScienceDirect

Solar Energy Materials & Solar Cells

journal homepage: www.elsevier.com/locate/solmat

# Study of the effect of annealing process on the performance of P3HT/PCBM photovoltaic devices using scanning-probe microscopy

Yu-Ching Huang [a], Yu-Chia Liao [a], Shao-Sian Li [a], Ming-Chung Wu [a], Chun-Wei Chen [a], Wei-Fang Su [a,b,*]

[a] Department of Materials Science and Engineering, National Taiwan University, Taipei 106-17, Taiwan
[b] Institute of Polymer Science and Engineering, National Taiwan University, Taipei 106-17, Taiwan

ARTICLE INFO

*Article history:*
Received 21 December 2007
Received in revised form
1 October 2008
Accepted 24 October 2008
Available online 21 December 2008

*Keywords:*
Photovoltaic
Scanning near-field microscopy
Atomic force microscopy
Anneal process

ABSTRACT

We have studied the effect of annealing process on the performance of photovoltaic devices based on the bulk heterojunction of poly(3-hexylthiophene) and [6,6]-phenyl-$C_{61}$ butyric acid methyl ester (P3HT/PCBM). By means of atomic force microscopy (AFM) and scanning of near-field microscopy (SNOM), we can observe the morphology evolution of the annealed P3HT/PCBM composite films. We also studied the changes of optical properties by absorption spectroscopy and the changes of composition distribution of annealed composite films. The results indicate the P3HT in the composite film gradually becomes an ordered structure with annealing. The ordered P3HT facilitates the charge transport. However, the film exhibits a large-scale (1 μm) PCBM aggregation after annealing for an extended period of time. The disrupted bi-continous phase retards the charge transport. Thus, the device efficiency reaches the highest (2.308%) after annealing at 140 °C for 30 min but decreases to 0.810% after 60 min annealing.



## 1. Introduction

Plastic solar cells have emerged as a promising cost-effective alternative to silicon-based solar cells. Some of the important advantages of these cells include ease of processing, mechanical flexibility, and low cost of fabrication. However, the efficiency of the plastic solar cell is too low for practical use at present. Recently, bulk heterojunction (BHJ) solar cells, obtained by blending conducting polymer (donor) and nanoparticles (acceptor) within a bulk [1–3], yield photovoltaic power conversion efficiency up to 4–5% [4–6]. The cells fabricated from regioregular poly(3-hexylthiophene) (P3HT) as the electron donor and [6,6]-phenyl-$C_{61}$ butyric acid methyl ester (PCBM) as the electron acceptor have shown the highest conversion efficiency in BHJ solar cells.

The efficiency of solar cells based on P3HT and PCBM depends strongly on the processing conditions, for example, solvent annealing [7] and thermal annealing [8–10]. Especially for thermal annealing, it is the most common way to improve cell efficiency. During thermal annealing, growth and perfection of polymer crystallization occurred, which increases the charge-transport capability. However, a prolonged annealing process will increase the crystallization of P3HT and force the aggregation of PCBM. Therefore, a large extent of phase separation will be observed, which reduces the bi-continuous phases present in the composite thin film and decreases its efficiency. The effect of blend morphology on polymer solar cell performance has been an important subject to be studied extensively in theoretical and experimental works [11–16].

We have used scanning-probe microscopy equipped with near-field spectroscopy (scanning of near-field microscopy (SNOM)) and Raman spectroscopy to study morphology changes upon heating to fully understand the mechanism of annealing and to optimize the annealing process. The SNOM is a novel and powerful technique that allows two-dimensional mapping of current and absorption in fully fabricated organic solar cells [17,18]. Some groups also use the SNOM to study optical and electronic properties in conjugated-polymer blends [19–21]. The SNOM is a scanning-probe technique in which a probe having a nanoscale aperture is held within the near-field of a sample surface. This permits the optical properties of a surface to be resolved at a length scale significantly smaller than the diffraction limit [22]. Moreover, we identify the phase separation by means of Raman spectroscopy.

## 2. Experimental details

In our experiment, the mixture of P3HT (Mw = 71,000 g mol$^{-1}$, PDI = 1.5, and regioregularity greater than 99% as determined by

* Corresponding author at: Department of Materials Science and Engineering, National Taiwan University, N1, Roosevelt Road, Section 4, Taipei 106-17, Taiwan. Tel./fax: +886 2 3366 4078.
*E-mail address:* suwf@ntu.edu.tw (W.-F. Su).

0927-0248/$ - see front matter © 2008 Elsevier B.V. All rights reserved.
doi:10.1016/j.solmat.2008.10.027

NMR, from Industrial Technology Research Institute, Taiwan) and PCBM (Aldrich Chemical) in 1:0.8 wt/wt ratio was dissolved in chlorobenzene and deposited by spin coat on the glass covered with 140-nm-thick layers of indium tin oxide (ITO) glass. The cathode of Al (~120 nm) was deposited on the blend layer by thermal deposition. The ITO glass substrate was ultrasonically cleaned in a series of organic solvents (ethanol, methanol, and acetone). A 40-nm-thick layer of PEDOT:PSS (Baytron P, 4083) was spin-coated to modify the ITO substrate surface at 200 rpm for 10 s and then at 4000 rpm for 60 s. After baking at 120 °C for 30 min in the oven, the substrates were transferred to a nitrogen-filled glove box (<0.1 ppm for $O_2$ and $H_2O$). The P3HT and PCBM were blended in a 1:0.8 wt/wt ratio, the blend was stirred for overnight at 50 °C in the glove box. The active layer was obtained by spin-coating at 700 rpm for 60 s. The thin film was dried in the covered glass Petri dishes. Al electrode was deposited on the thin film by thermal evaporation. The devices were annealed at 140 °C for different times and then the device was encapsulated with UV adhesive in $N_2$ atmosphere and tested in air.

The performance of these devices was evaluated under AM 1.5 G irradiation (100 mW $cm^{-2}$) using a solar simulator (Oriel Inc.). The evolution of surface morphology was studied by atomic force microscopy (AFM) (Digital Instruments, Nanoscope III). The film thickness was determined by an α-stepper (Veeco, Dektak 6M 24383). The UV-visible spectroscopy of the blends under different annealing processing was obtained by UV–visible absorption (Perkin Elmer Lambda 35). The nanoscale optical properties of the blend film were studied in the transmission mode using the scanning near-field optical microscopy (SNOM, WITec, AlphaSNOM, Germany) head with a special probe. The special probe with micro-fabricated cantilever SNOM sensors (aperture ~100 nm) exhibits high transmission efficiency; the argon ion laser (488 nm) was employed as radiation sources. The transmitted light was collected with a 40× objective and detected with a single photon counting photomultiplier tube. For each line scan, 256 data points were taken with a line scan frequency of 0.5 Hz. Raman spectra were collected with a Confocal Raman Microscope (WITec, CMR 200, Germany) in backscattering mode. In all cases, the laser beam was focused down with a 100× NA ~0.95 objective (Olympus, IX-70) in the inverted optical microscope. Optical resolution diffraction limited to 200 nm laterally and 500 nm vertically spectral resolution down to 0.02 wave numbers. A thermoelectrically cooled CCD Camera (Peltier cooler), with 1024 × 127 pixels, was operated at −60 °C for data acquisition. The acquisition time was fixed at 0.5 s for Raman mapping and at 20 s for single-spectra measurements.

## 3. Results and discussion

The absorption spectra of pristine P3HT and pristine PCBM and P3HT/PCBM composite thin films, which are annealed at 140 °C for different times, are shown in Fig. 1. The absorption of pristine P3HT is doubled after 10 min annealing, and then is increased gradually with increasing annealing time. Since the absorption band is the characteristic peak of the $\pi-\pi^*$ transition of the P3HT backbone, the increase in the absorption intensity is due to the increased $\pi-\pi$ stacking of the P3HT molecule with high chain ordering. In the case of PCBM, a decrease in absorption occurs after annealing for 60 min, which may be due to the aggregation of $C_{60}$. The change of absorption spectra of P3HT/PCBM composite films with annealing time is the combined spectra of pristine P3HT and pristine PCBM. The results indicate the annealing process increases the absorption of P3HT/PCBM composite films, which increases the device efficiency.

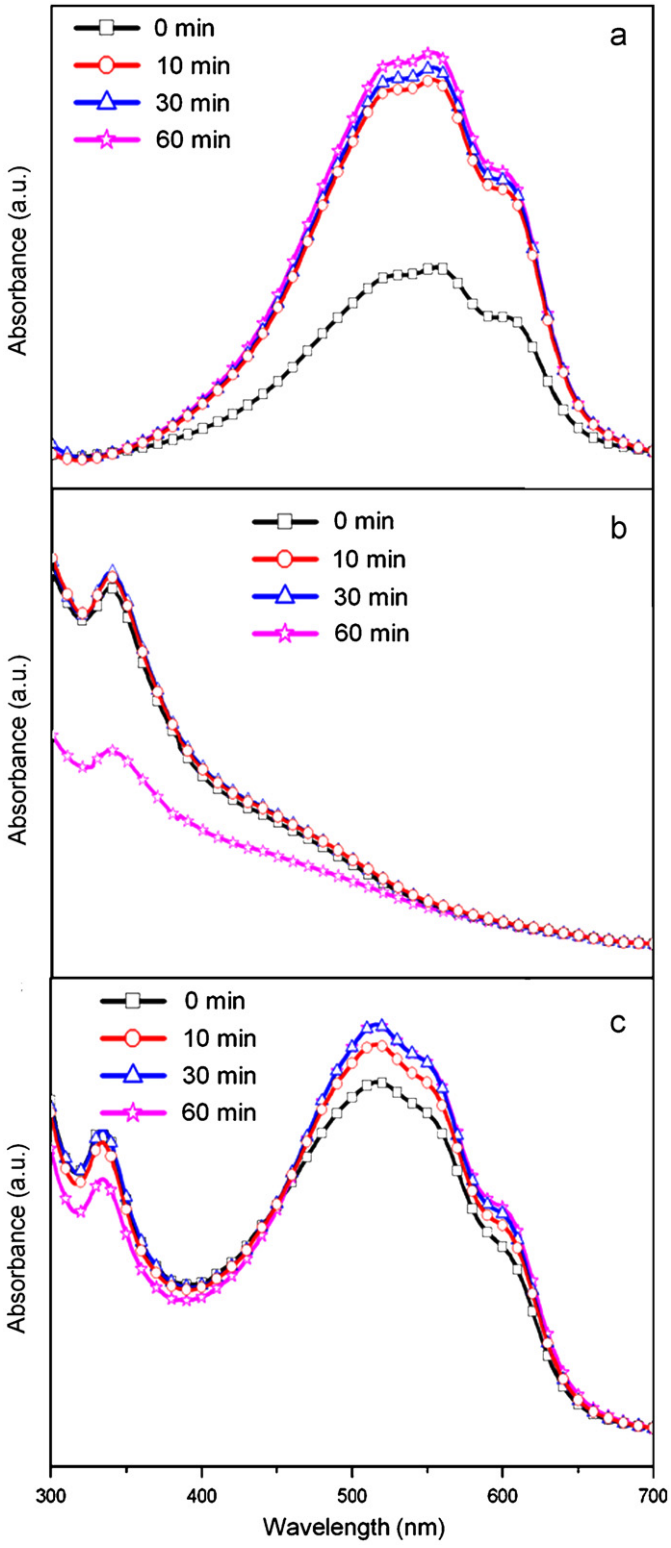


**Fig. 1.** Normalized absorption spectra of pristine P3HT (a), PCBM (b), and P3HT/PCBM composite thin films (c) after annealing at 140 °C for 0 min (-□-), 10 min (-○-), 30 min (-△-), and 60 min (-☆-).

In order to understand fully the changes of absorption characteristics after the thermal aging of P3HT/PCBM composite films, we have used SNOM to study the absorption changes in nanoscale. In a near-field optical measurement, a SNOM probe with a hole of around 100 nm in diameter on the sharp end is

placed into the near-field of the investigated sample. The spatial resolution is then defined by the diameter of the hole. High-quality optical contrast images were obtained by this technique. It is an important technique to analyze the optical properties of nanomaterials. Fig. 2 shows the results of SNOM studies, including samples without annealing and annealing for 60 min. Fig. 2c shows a homogeneous absorption for the sample without annealing. After annealing at 140 °C for 60 min, the absorption of the sample became stronger than that of without annealing and the corresponding topographic images show a dramatic increase in surface roughness (Fig. 2b and d). The results are consistent with the absorption study of the annealed samples as shown in Fig. 1. For the sample annealed for 60 min, a large extent of aggregation was observed as shown in Fig. 2b. This large aggregation blocked the light and decreased the absorption in aggregated regions. The result has been revealed in the absorption spectrum of the PCBM (Fig. 1b). Therefore, we hypothesize the formation of aggregation is PCBM. We have used confocal Raman spectroscopy to identify the composition of the aggregates. The results are discussed after the discussion of the AFM study.

In order to observe the morphology evolution much clearly, we have used the AFM to monitor the evolution of morphology of P3HT/PCBM composite thin films with annealing processing. The results are shown in Fig. 3. The film without annealing has a very smooth surface with r.m.s. roughness of 1.5 nm. After 10 min of annealing at 140 °C, the roughness of the film increases a little. The low extent of surface roughness growth will effectively reduce the charge-transport distance, increase the current density [6], enhance internal light scattering and light absorption, as shown in their UV-vis absorption spectra (Fig. 1). The surface roughness increases with increasing annealing time, and then it becomes very rough after 60 min of annealing. The rough surface is due to the aggregation of PCBM. After a long period of annealing, the P3HT becomes soft, and the PCBM will float on the surface and form large aggregates gradually.

We have used confocal Raman spectroscopy to identify the aggregates are PCBM. Fig. 4 shows the confocal images of the P3HT/PCBM composite thin films, which are annealed at 140 °C for different times. From these confocal images, we can observe the aggregates become larger with an increase in annealing time. Many bright spots are formed after 60 min annealing as shown in

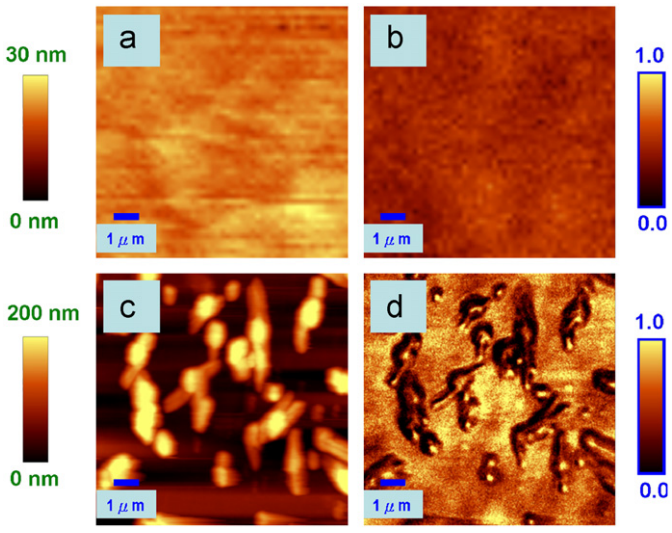


**Fig. 2.** SNOM images under transmission mode using monochromatic laser radiation 488 nm of P3HT/PCBM systems. (a,b) are topographic images after annealing at 140 °C for 0 and 60 min. (c,d) are SNOM images after annealing at 140 °C for 0 and 60 min.

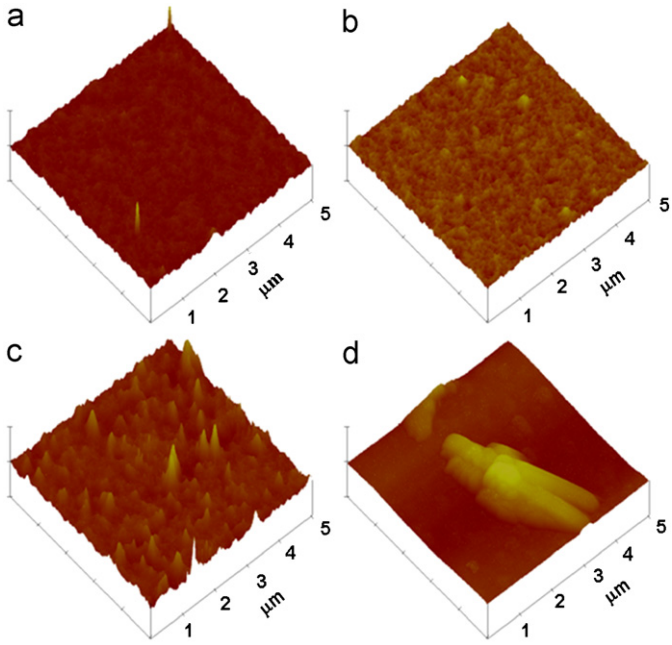


**Fig. 3.** 3-D topography images of P3HT/PCBM composite thin films after different annealing times at 140 °C: (a) without annealing, (b) 10 min, (c) 30 min, and (d) 60 min.

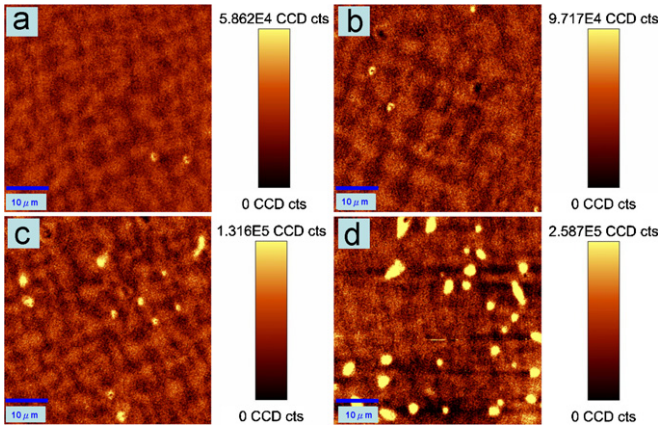


**Fig. 4.** Confocal images of P3HT/PCBM composite thin films after annealing process at 140 °C for (a) 0 min, (b) 10 min, (c) 30 min, and (d) 60 min.

Fig. 4d and its corresponding Raman spectrum is shown in Fig. 5. From the literature [23], the intensive Raman bands of P3HT at 1440 and 1380 $cm^{-1}$ are due to the C = C stretching vibrations of the thiophene ring and C–C skeletal stretching. Another Raman band of P3HT at 728 $cm^{-1}$ is assigned to the deformation vibration of the C–S–C bond. For the PCBM, a strong Raman signal is detected, which covers a broad range of 1500–3000 $cm^{-1}$. From Fig. 5, the bright area contains both P3HT and PCBM Raman bands (Fig. 5c). However, the dark area contains the P3HT Raman band only (Fig. 5b). We can conclude that the dark area is the P3HT-rich region and the bright area is the PCBM-rich region. The long annealing time causes the P3HT to flow and the PCBM to aggregate, which resulted in a large extent of phase separation and the disruption of bi-continuous phases.

Fig. 6 shows the *I–V* characteristic curves of the solar cell made of P3HT/PCBM composite films annealed at 140 °C for different times under A.M. 1.5 illuminations. The thickness of the films is all

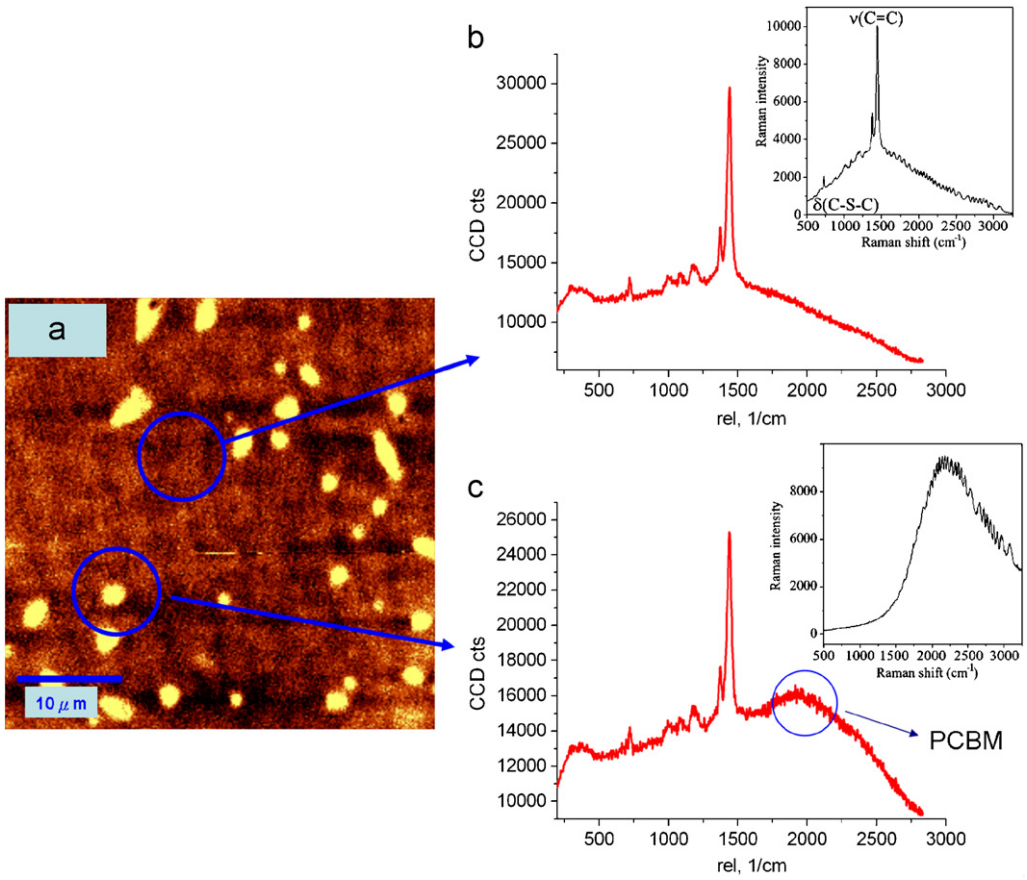


**Fig. 5.** Topography (a) and Raman spectra of P3HT/PCBM composite thin films after annealing process at 140 °C for 60 min. The darker region shows Raman band of P3HT (b) only, and the brighter region exhibits the Raman band of PCBM (c) in addition to P3HT.

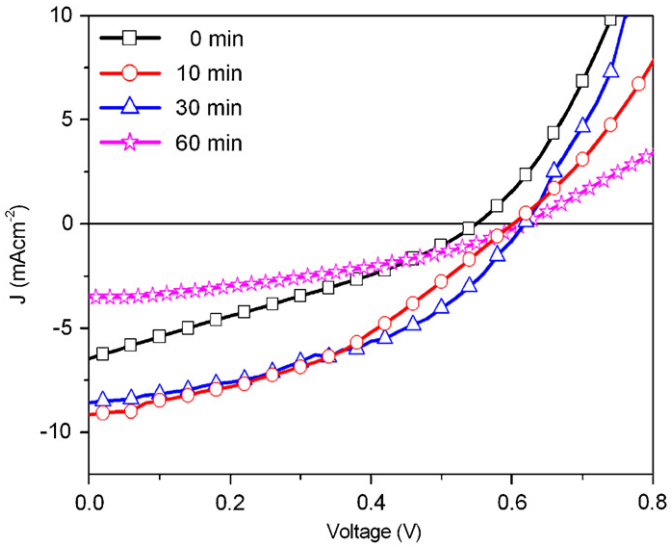


**Fig. 6.** IV characteristics of photovoltaic devices based on P3HT/PCBM composite films with annealing at 140 °C for different times under A.M. 1.5 illuminations (100 mW cm$^{-2}$).

kept around 100 nm. The performance of the solar cell efficiency improves with annealing time from 0 to 30 min. The results are due to the increased light absorption (Fig. 1c) and the small extent of PCBM aggregation (Figs. 2 and 3). The PCBM-rich region reduces the recombination losses and increases the current density [24,25]; thus, the performance of solar cell is increased after annealing. However, the annealing process at 140 °C for 60 min decreases the performance of the solar cell. The formation of the large area of PCBM aggregates increases the chance of short-circuit formation and results in poor device performance. Table 1 shows the performance results of solar cells annealed at 140 °C for different times. The best performance of solar cell is made by annealing at 140 °C for 30 min with an efficiency of 2.308% under A.M. 1.5 illuminations.

**Table 1**
Performance of P3HT/PCBM composite solar cell under A.M. 1.5 illuminations (100 mW cm$^{-2}$) with annealing at 140 °C for different times.

| Annealing time (min) | $V_{oc}$ (V) | $J_{sc}$ (mA cm$^{-2}$) | FF (%) | $\eta$ (%) |
|---|---|---|---|---|
| 0 | 0.548 | 6.463 | 29.35 | 1.039 |
| 10 | 0.600 | 9.135 | 39.86 | 2.185 |
| 30 | 0.616 | 8.584 | 43.65 | 2.308 |
| 60 | 0.616 | 3.501 | 37.54 | 0.810 |

## 4. Conclusions

We have studied the effect of annealing process on the performance of P3HT/PCBM photovoltaic devices. The results of UV–vis, AFM, and SNOM studies reveal that the P3HT of the composite film becomes an ordered structure gradually up to 30 min at 140 °C. However, a large-scale (1 μm) PCBM aggregation

was identified by confocal Raman spectroscopy, which occurred after the film annealed at 140 °C for 60 min. The ordered structure facilitates the charge transport and the large aggregation disrupts the process. Thus, the device efficiency increases from 1.039% to 2.308% after annealing at 140 °C for 30 min, then decreases to 0.810% with 60 min annealing.

## Acknowledgements

The financial support from the National Science Council of Taiwan (NSC-96-2628-E-002-017-MY3 and NSC 95-3114-P-002-003-MY3) is highly appreciated. The authors would also like to thank Mr. Y.Y. Lin of National Taiwan University for helpful discussions.

## References

[1] G. Yu, J. Gao, J.C. Hummelen, F. Wudl, A.J. Heeger, Polymer photovoltaic cells: enhanced efficiencies via a network of internal donor–acceptor heterojunctions, Science 270 (1995) 1789–1791.
[2] M. Granstrom, K. Petrisch, A.C. Arias, A. Lux, M.R. Andersson, R.H. Friend, Laminated fabrication of polymeric photovoltaic diodes, Nature 395 (1998) 257–260.
[3] C.J. Brabec, N.S. Sariciftci, J.C. Hummelen, Plastic solar cells, Adv. Funct. Mater. 11 (2001) 15–26.
[4] L.S. Roman, M.R. Andersson, T. Yohanms, O. Inganas, Photodiode performance and nanostructure of polythiophene/$C_{60}$ blends, Adv. Mater. 9 (1997) 1164–1168.
[5] C.J. Brabec, S.E. Shaheen, C. Winder, N.S. Sariciftci, P. Denk, Effect of LiF/metal electrodes on the performance of plastic solar cells, Appl. Phys. Lett. 80 (2002) 1288–1290.
[6] G. Li, V. Shrotriya, J. Huang, Y. Yao, K. Emery, Y. Yang, High-efficiency solution processable polymer photovoltaic cells by self-organization of polymer blends, Nat. Mater. 4 (2005) 864–868.
[7] G. Li, Y. Yao, H. Yang, V. Shrotriya, G. Yang, Y. Yang, Solvent annealing effect in polymer solar cells based on poly(3-hexylthiophene) and methanofullerenes, Adv. Funct. Mater. 17 (2007) 1636–1644.
[8] F. Padinger, R.S. Rittberger, N.S. Sariciftci, Effects of postproduction treatment on plastic solar cells, Adv. Funct. Mater. 13 (2003) 85–88.
[9] X.N. Yang, J.K.J. Van Duren, M.T. Rispens, J.C. Hummelen, R.A.J. Janssen, M.A.J. Michels, J. Loos, Crystalline organization of a methanofullerene as used for plastic solar-cell applications, Adv. Mater. 16 (2004) 802–806.
[10] N. Camaioni, G. Ridolfi, G. Casalbore-Miceli, G. Possamai, M. Maggini, The effect of a mild thermal treatment on the performance of poly(3-alkylthiophene)/fullerene solar cells, Adv. Mater. 14 (2002) 1735–1738.
[11] B.A. Gregg, M.C. Hanna, Comparing organic to inorganic photovoltaic cells: theory, experiment, and simulation, J. Appl. Phys. 93 (2003) 3605–3614.
[12] B.A. Gregg, Excitonic solar cells, J. Phys. Chem. B 107 (2003) 4688–4698.
[13] A.C. Arias, J.D. Mackenzie, R. Stevenson, J.M. Halls, M. Inbasekaran, P.E. Woo, D. Richards, R.H. Friend, Photovoltaic performance and morphology of polyfluorene blends: a combined microscopic and photovoltaic investigation, Macromalecules 34 (2001) 6005–6013.
[14] J.M. Halls, A.C. Arias, J.D. Mackenzie, W. Wu, M. Inbasekaran, P.E. Woo, D. Richards, R.H. Friend, Photodiodes based on polyfluorene composites: influence of morphology, Adv. Mater. 12 (2000) 498–502.
[15] H.J. Snaith, A.C. Arias, A.C. Morteani, C. Silva, R.H. Friend, Charge generation kinetics and transport mechanisms in blended polyfluorene photovoltaic devices, Nano Letters 2 (2002) 1353–1357.
[16] E.J. Moons, Conjugated polymer blends: linking film morphology to performance of light emitting diodes and photodiodes, J. Phys.: Condens. Matter 14 (2002) 12235–12260.
[17] C.R. Mcneill, H. Frohne, J.L. Holdsworth, J.E. Furst, B.V. King, P.C. Dastoor, Direct photocurrent mapping of organic solar cells using a near-field scanning optical microscope, Nano Letters 4 (2004) 219–223.
[18] C.R. Mcneill, H. Frohne, J.L. Holdsworth, P.C. Dastoor, Near-field scanning photocurrent measurements of polyfluorene blend devices: directly correlating morphology with current generation, Nano Letters 4 (2004) 2503–2507.
[19] H. Aoki, Y. Kunai, S. Ito, H. Yamada, K. Matsushige, Two-dimensional phase separation of block copolymer and homopolymer blend studied by scanning near-field optical microscopy, Appl. Surf. Sci. 188 (2002) 534–538.
[20] P.F. Barbara, D.M. Adams, D.B. O'Conner, Characterization of organic thin film materials with near-field scanning optical microscopy, Annu. Rev. Mater. Sci. 29 (1999) 433–469.
[21] A. Cadby, R. Dean, A.M. Fox, R.A.L. Jones, D.G. Lidzey, Mapping the fluorescence decay lifetime of a conjugated polymer in a phase-separated blend using a scanning near-field optical microscope, Nano Letters 5 (2005) 2232–2237.
[22] E. Hecht, Optics, third ed., Addison-Wesley, Reading, MA, 1998.
[23] E. Klimov, W. Li, X. Yang, G.G. Hoffmann, J. Loos, Scanning near-field and confocal raman microscopic investigation of P3HT-PCBM systems for solar cell applications, Macromolecules 39 (2006) 4493–4496.
[24] M. Reyes-Reyes, K. Kim, D.J. Carroll, High-efficiency photovoltaic devices based on annealed poly(3-hexylthiophene) and 1-(3-methoxycarbonyl)-propyl-1-phenyl-(6,6)$C_{61}$ blends, Appl. Phys. Lett. 87 (2005) 083506.
[25] R. Shilkler, M. Chiesa, R.H. Friend, Photovoltaic performance and morphology of polyfluorene blends: the influence of phase separation evolution, Marcomolecules 39 (2006) 5393–5399.